Investigation of buckling behavior of functionally graded piezoelectric (FGP) rectangular plates under open and closed circuit conditions

M.A. Ghasemabadian[a] and M. Kadkhodayan[*]

Department of Mechanical Engineering, Ferdowsi University of Mashhad, Mashhad, Iran

Abstract. In this article, based on the higher-order shear deformation plate theory, buckling analysis of a rectangular plate made of functionally graded piezoelectric materials and its effective parameters are investigated. Assuming the transverse distribution of electric potential to be a combination of a parabolic and a linear function of thickness coordinate, the equilibrium equations for the buckling analysis of an FGP rectangular plate are established. In addition to the Maxwell equation, all boundary conditions including the conditions on the top and bottom surfaces of the plate for closed and open circuited are satisfied. Considering double sine solution (Navier solution) for displacement field and electric potential, an analytical solution is obtained for full simply supported boundary conditions. The accurate buckling load of FGP plate is presented for both open and closed circuit conditions. It is found that the critical buckling load for open circuit is more than that of closed circuit in all loading conditions. Furthermore, it is observed that the influence of dielectric constants on the critical buckling load is more than those of others.

Keywords: buckling; functionally graded piezoelectric; rectangular plate; dielectric constants; piezoelectric constants; analytical solution

1. Introduction

Functionally graded piezoelectric materials (FGPMs) are a new type of intelligent materials which have been used in micro-electro-mechanical systems (MEMs) and smart structures as actuators and sensors (2008b). Because of important applications in medical and aerospace industry, these materials have attracted attentions in researches. FGPMs have material properties which vary spatially from a point to another point continuously. The buckling analysis of plates, shells and beams is one of the most important research fields on isotropic, composite materials, functionally graded FGMs, piezoelectric materials and FGPMs.

In the case of isotropic and composite materials many researchers have been considered buckling analysis. For example, Kuo and Yau (2012) derived buckling equations of orthotropic thin plates using energy approaches. Hosseini-Hashemi *et al.* (2008a) studied the buckling analysis

---

∗Corresponding author, Professor , E-mail: kadkhoda@um.ac.ir
[a]Ph.D. Student, E-mail: ghasemabadian@stu.um.ac.ir

of in plane loaded isotropic rectangular plates with Levy-type boundary conditions and obtained an analytical closed-form solution. Civalek *et al.* (2010c) using classical plate theory studied the buckling analysis of rectangular plates subjected to various uniform and non-uniform distributed in-plane compressive loads. The buckling analysis of thin isotropic plates and columns by using differential quadrature (DQ) and harmonic differential quadrature (HDQ) was presented by Civalek (2004a). Using variable refined plate theory, Kim *et al.* (2009c) investigated the buckling analysis of isotropic and orthotropic simply supported rectangular plates.

For the buckling analysis of functionally graded rectangular plates, based on classical plate theory, Javaheri and Eslami studied the buckling analysis of simply supported plate under mechanical (2002a) and thermal (2002b) loadings. Moreover, Shariat and Eslami (2007) presented a closed form solution for the buckling analysis of simply supported plate based on higher order shear deformation plate theory under mechanical and thermal loadings. The thermal buckling analysis of simply supported plates based on first and third order shear deformation theory was investigated by Lanhe (2004b) and Javaheri and Eslami (2002b), respectively. The critical buckling load for the plate with Levy-type boundary conditions based on classical, first and third order shear deformation theory was presented by Mohammadi *et al.* (2010e), (2010d) and Bodaghi and Saidi (2010b), respectively. Based on classical plate theory, Amiri Rad and Panahandeh-Shahraki (2014d) investigated the critical buckling load of plates containing a crack. Moreover, Akgöz and Civalek (2014a) investigated the thermo-mechanical size-dependent buckling analysis of functionally graded micro-beams based on the sinusoidal shear deformation beam and modified couple stress theories.

On the other hand, the buckling and post-buckling analysis of piezoelectric plates, have been addressed by many researchers and several works have been conducted to investigate the buckling, post-buckling and thermal buckling behaviors of smart composite plates. For instance, buckling control of laminated composite plates using piezoelectric materials on the basis of the first order shear deformation plate theory was studied by Chandrashekhara and Bathia (1993). Based on the three-dimensional elasticity theory, the dynamic buckling analysis of a plate with surface bonded piezoceramic elements was presented by Batra and Geng (2001a). Varelis and Saravanos (2004c) presented the buckling and post-buckling response of composite laminates and plates with piezo-actuators and sensors due to large displacements and rotations.

Dynamic buckling of laminated plates with piezoelectric sensors and actuators under thermo-electro-mechanical loadings was studied by Shariyat (2009d, 2009e). Based on higher order shear deformation plate theory, he investigated the forced and free vibration and dynamic buckling of rectangular FG plates with piezoelectric sensors and actuators subjected to thermo-electro-mechanical loading conditions. Three-dimensional thermal buckling analysis of simply-supported piezoelectric asymmetric angle-ply laminates with finite layer method studied by Akhras and Li (2010a). Yang (1998) obtained equations for the buckling of a thin piezoelectric plate and showed that the effect of piezoelectricity on the buckling load is of the order of the electro-mechanical coupling factor which is not small when the material has a strong piezoelectric coupling. Based on the higher order shear deformation plate theory, Shen (2005, 2009f) presented the thermal post-buckling analysis of a simply supported laminated plate with piezoelectric actuators subjected to the thermo-electrical and the thermo-electro-mechanical loads. He (2001b) studied the post-buckling analysis of simply supported, symmetric FG plates with fully covered or embedded piezoelectric actuators subjected to the thermo-electro-mechanical loads. Moreover, he presented a fully nonlinear compressive post-buckling and thermal post-buckling analysis for FG hybrid plates with PFRC actuators (2001c). A three-dimensional exact piezoelasticity solution for buckling of

simply-supported symmetrically laminated hybrid plates with piezoelectric layers was presented by Kapuria and Achary (2006b). Using three-dimensional state-space formulations, influence of weak interfaces on the buckling of simply supported orthotropic piezoelectric laminates with interlaminar bonding imperfections was investigated by Kim and Lee (2008b). Moreover, Jadhav and Bajoria (2013b) based on the first order shear deformation plate theory investigated the stability analysis of FGM plate with two piezoelectric layers using finite element method.

The buckling delamination problem of a simply supported sandwich plate-strip with a piezoelectric face and elastic core layers was studied by Akbarov and Yahnioglu (2013a). In order to investigate the effect of stored voltage in actuators, Panahandeh-Shahraki *et al.* (2014c) presented fully coupled electromechanical buckling analysis of thin to thick active laminated composites. Fereidoon *et al.* (2014b) introduced an analytical approach for buckling analysis of two layered FGMs that were integrated with surface-bonded piezoelectric actuators subjected to thermo-electro-mechanical loads. Mirzavand and Eslami (2011a) presented a close-form solution for the thermal buckling of functionally graded plates with piezoelectric actuators subjected to thermo-electrical loadings.

Finally, buckling analysis of thick functionally graded piezoelectric rectangular plates was investigated based on the higher-order shear and normal deformable plate theory by Abdollahi *et al.* (2015). They considered two cases consisting of closed and open–closed circuits as electrical conditions.

Contrary to functionally graded and piezoelectric materials, there are not so many researches on the buckling analysis of functionally graded piezoelectric plates. Although some studies achieved on the buckling of FGPMs referred to buckling analysis of cylindrical shells (2010f) and thick plates (2015), but analysis of the effect of piezoelectric constants on buckling behavior of plates and shells is still an open area and needs more attentions.

According to the all-around literature review, it can be found that there is no work on the investigation of piezoelectric constants effect on the buckling behavior of a rectangular plate made of FGPM. In this study, based on third order shear deformation plate theory, the buckling analysis of simply supported rectangular functionally graded piezoelectric plates for both open and closed circuited electrical conditions are investigated. Assuming the function of electric potential is a combination of parabolic and linear functions of thickness coordinate z, the Maxwell equation and all boundary conditions including the conditions on the top and bottom surfaces of the plate for closed and open circuited are satisfied.

Considering the principle of minimum total potential energy, the equilibrium equations of the plate are derived. By using double series solution, six coupled governing partial differential equations are solved and the accurate critical buckling load is obtained. Verifying the accuracy of the present solution a comparison is performed for a special case of the functionally graded piezoelectric plate without piezoelectric effects. Finally, the effects of plate thickness, piezoelectric constants, piezoelectric index, loading conditions and circuited electrical conditions for some different FGPMs are comprehensively investigated.

2. Geometry and material properties

Consider a flat rectangular plate with the length *a*, width *b*, thickness *h*. The plate is made of FGPM with material properties varying spatially through the thickness direction continuously according to a power law distribution expressed as

$$\Theta(z) = \Theta_b + (\Theta_t - \Theta_b)\left(\frac{1}{2} - \frac{z}{h}\right)^n \tag{1}$$

where n is the material power law index and Θ_b and Θ_t denote the material property of the bottom $\left(z = -\frac{h}{2}\right)$ and top $\left(z = \frac{h}{2}\right)$ surfaces of the plate, respectively. In this study, Θ demonstrates FGPM properties such as the elastic (C_{ij}), piezoelectric (e_{ij}) and dielectric constants (Ξ_{ij}). It should be mentioned that FGP is polarized perpendicular to the mid-plane in the direction of the *z*-axis.

3. Equilibrium and stability equations

Considering the third-order shear deformation plate theory (2010b) and the von-Karman hypothesis for non-linear relation of strain–displacement (2010b), the linear constitutive relations describing the electrical and mechanical interaction of FGPMs in the plane stress state can be written as (2010f)

$$\begin{Bmatrix} \sigma_{xx} \\ \sigma_{yy} \\ \sigma_{xy} \\ \sigma_{xz} \\ \sigma_{yz} \end{Bmatrix} = \begin{bmatrix} \bar{C}_{11} & \bar{C}_{12} & 0 & 0 & 0 \\ \bar{C}_{12} & \bar{C}_{11} & 0 & 0 & 0 \\ 0 & 0 & (\bar{C}_{11} - \bar{C}_{12})/2 & 0 & 0 \\ 0 & 0 & 0 & C_{55} & 0 \\ 0 & 0 & 0 & 0 & C_{55} \end{bmatrix} \begin{Bmatrix} \varepsilon_{xx} \\ \varepsilon_{yy} \\ \gamma_{xy} \\ \gamma_{xz} \\ \gamma_{yz} \end{Bmatrix} - \begin{bmatrix} 0 & 0 & \bar{e}_{31} \\ 0 & 0 & \bar{e}_{31} \\ 0 & 0 & 0 \\ e_{15} & 0 & 0 \\ 0 & e_{15} & 0 \end{bmatrix} \begin{Bmatrix} E_x \\ E_y \\ E_z \end{Bmatrix}$$

$$\begin{Bmatrix} D_x \\ D_y \\ D_z \end{Bmatrix} = \begin{bmatrix} 0 & 0 & 0 & e_{15} & 0 \\ 0 & 0 & 0 & 0 & e_{15} \\ \bar{e}_{31} & \bar{e}_{31} & 0 & 0 & 0 \end{bmatrix} \begin{Bmatrix} \varepsilon_{xx} \\ \varepsilon_{yy} \\ \gamma_{xy} \\ \gamma_{xz} \\ \gamma_{yz} \end{Bmatrix} + \begin{bmatrix} \Xi_{11} & 0 & 0 \\ 0 & \Xi_{11} & 0 \\ 0 & 0 & \bar{\Xi}_{33} \end{bmatrix} \begin{Bmatrix} E_x \\ E_y \\ E_z \end{Bmatrix} \tag{2}$$

Where $[C]$ is the reduced stiffness matrix at constant electric field, $[e]$ is the reduced matrix of piezoelectric constants, $[\Xi]$ is dielectric constants matrix, $\{E\}$ is the electric field and $\{D\}$ is electric displacement field. In order to satisfy the Maxwell equation and the electrical conditions for open and closed circuits, the transverse distribution for electric potential is proposed as

$$\Phi(x,y,z) = \left(1 - \frac{4z^2}{h^2}\right)\phi(x,y) + A(x,y)z + B(x,y) \tag{3}$$

Where ϕ is the electric potential on the mid-surface of the FGP layer and A and B are determined through satisfying the electrical boundary conditions on the surfaces of FGP plate. Moreover, based on the linear piezoelectricity, the electric field is the gradient of electric potential as

$$E_x = -\Phi_{,x}, \qquad E_y = -\Phi_{,y}, \qquad E_z = -\Phi_{,z} \tag{4}$$

when both surfaces of the plate are short-circuited, the electrical boundary conditions for a closed circuit piezoelectric layer are represented as

$$\Phi(x,y,\pm h/2)=0 \qquad (5)$$

On the other hand, when the inner surface of the plate is held at zero voltage and the outer surface is in contact with a low permittivity medium such as air or vacuum (open circuit condition), the following surface boundary conditions are assumed

$$\Phi(x,y,-h/2)=0, \qquad D_z(x,y,h/2)=0 \qquad (6)$$

Applying the principle of minimum total potential energy, the equilibrium equations are obtained as

$$N_{xx,x}+N_{xy,y}=0$$

$$N_{xy,x}+N_{yy,y}=0$$

$$M_{xx,x}+M_{xy,y}-Q_{xz}-\alpha\left(P_{xx,x}+P_{xy,y}\right)+\beta R_x=0$$

$$M_{xy,x}+M_{yy,y}-Q_{yz}-\alpha\left(P_{xy,x}+P_{yy,y}\right)+\beta R_y=0$$

$$Q_{xz,x}+Q_{yz,y}+\alpha\left(P_{xx,xx}+2P_{xy,xy}+P_{yy,yy}\right)-\beta\left(R_{x,x}+R_{y,y}\right)$$

$$+N_{xx}w_{,xx}+2N_{xy}w_{,xy}+N_{yy}w_{,yy}=0 \qquad (7)$$

where subscripts (,) denotes the differentiation with respect to the Cartesian coordinate and $\beta=3\alpha=4/h^2$ and N_i, M_i, P_i ($i=xx,\ yy,\ xy$) are the resultant forces, moments and higher-order moments, respectively, and Q_i, R_i ($i=xz,\ yz$) are the shear and higher-order shear forces, respectively, defined by following relations (2010b)

$$\left(N_i,M_i,P_i\right)=\int_{-h/2}^{h/2}\sigma_i\left(1,z,z^3\right)dz,\ \ (i=xx,\ yy,\ xy)$$

$$\left(Q_i,R_i\right)=\int_{-h/2}^{h/2}\sigma_i\left(1,z^2\right)dz,\ \ (i=xz,\ yz) \qquad (8)$$

According to the adjacent equilibrium criterion for obtaining the stability equations of buckling, a neighboring state of equilibrium is considered as an increment in the displacement field (1979, 2006a, 2011b). Therefore, the displacement field can be written as

$$u\to u^0+u^1,\ \ v\to v^0+v^1\ \ w\to w^0+w^1,\ \ \psi_x\to\psi_x^{\ 0}+\psi_x^{\ 1}\ \ \psi_y\to\psi_y^{\ 0}+\psi_y^{\ 1} \qquad (9)$$

where the arrow is read "be replaced by" and superscripts "0" and "1" refer to equilibrium and neighboring states, respectively. Moreover, w is the transverse displacement and ψ_x and ψ_y are rotation functions of the middle surface in the x and y directions, respectively, and u and v are the mid-plane displacements of the plate in the x and y directions, respectively.

Substitution of the relations (9) into (8), the expressions for stress resultants related to the equilibrium and neighboring states are obtained as follows

$$\left(N_i,M_i,P_i\right)\to\left(N_i^{\ 0},M_i^{\ 0},P_i^{\ 0}\right)+\left(N_i^{\ 1},M_i^{\ 1},P_i^{\ 1}\right),\ \ (i=xx,\ yy,\ xy)$$

$$\left(Q_i,R_i\right)\to\left(Q_i^0,R_i^0\right)+\left(Q_i^1,R_i^1\right),\ \ \ (i=xz,\ yz) \qquad (10)$$

where the terms with superscripts 0 related to the equilibrium conditions and those with superscripts 1 are linear parts of the stress resultants increments corresponding to the neighboring state. Substituting relations (10) into Eqs. (7), the terms in the resulting equations with superscript 0 are omitted because of satisfying the equilibrium conditions. Moreover, the non-linear terms with superscript 1 are ignored because of the smallness of the incremental displacement compared to the linear terms. The remaining terms form the stability equations as

$$N^1_{xx,x} + N^1_{xy,y} = 0$$

$$N^1_{xy,x} + N^1_{yy,y} = 0$$

$$M^1_{xx,x} + M^1_{xy,y} - Q^1_{xz} - \alpha\left(P^1_{xx,x} + P^1_{xy,y}\right) + \beta R^1_x = 0$$

$$M^1_{xy,x} + M^1_{yy,y} - Q^1_{yz} - \alpha\left(P^1_{xy,x} + P^1_{yy,y}\right) + \beta R^1_y = 0$$

$$Q^1_{xz,x} + Q^1_{yz,y} + \alpha\left(P^1_{xx,xx} + 2P^1_{xy,xy} + P^1_{yy,yy}\right) - \beta\left(R^1_{x,x} + R^1_{y,y}\right) + N^0_{xx}w^1_{,xx} +$$
$$2N^0_{xy}w^1_{,xy} + N^0_{yy}w^1_{,yy} = 0 \tag{11}$$

where $N^0_i, (i = xx, xy, yy)$ can be replaced by the pre-buckling forces obtained from equilibrium conditions. The above equations formed the stability equations of the plate subjected to the in-plane edge loading. Besides mentioned equations, the variables should also satisfy the Maxwell equation which requires that the divergence of the electric flux density vanishes at any point within the media. In order to satisfy this condition, the integration of the electric flux divergence across the thickness of the piezoelectric layers must be zero for any x and y as (2009a)

$$\int_{-h/2}^{h/2} \left(\frac{\partial D_x}{\partial x} + \frac{\partial D_y}{\partial y} + \frac{\partial D_z}{\partial z}\right) dz = 0 \tag{12}$$

Substituting relations of displacement and strains into Eqs. (10) and (11) the governing stability equations are obtained as

$$A_1\left(w^1_{,xxx} + w^1_{,xyy}\right) + A_2\psi^1_{x,xx} + A_3\psi^1_{x,yy} + A_4\psi^1_{y,xy} + A_5u^1_{,xx} +$$
$$A_6u^1_{,yy} + A_7v^1_{,xy} + A_8\phi_{,x} = 0$$

$$A_1\left(w^1_{,xxy} + w^1_{,yyy}\right) + A_2\psi^1_{y,yy} + A_3\psi^1_{y,xx} + A_4\psi^1_{x,xy} + A_5v^1_{,yy} +$$
$$A_6v^1_{,xx} + A_7u^1_{,xy} + A_8\phi_{,y} = 0$$

$$B_1\left(w^1_{,xxx} + w^1_{,xyy}\right) + B_2\psi^1_{x,xx} + B_3\psi^1_{x,yy} + B_4\psi^1_{y,xy} + B_5u^1_{,xx} + B_6u^1_{,yy} +$$
$$B_7v^1_{,xy} + B_8\left(w^1_{,x} + \psi^1_x\right) + B_9\phi_{,x} = 0$$

$$B_1\left(w^1_{,xxy} + w^1_{,yyy}\right) + B_2\psi^1_{y,yy} + B_3\psi^1_{y,xx} + B_4\psi^1_{x,xy} + B_5v^1_{,yy} + B_6v^1_{,xx} +$$
$$B_7u^1_{,xy} + B_8\left(w^1_{,y} + \psi^1_y\right) + B_9\phi_{,y} = 0$$

$$D_1\left(w^1_{,xxxx} + 2w^1_{,xxyy} + w^1_{,yyyy}\right) + D_2\left(\psi^1_{x,xxx} + \psi^1_{x,xyy} + \psi^1_{y,yxx} + \psi^1_{y,yyy}\right) +$$

$$D_3\left(u^1_{,xxx} + u^1_{,xyy} + v^1_{,yxx} + v^1_{,yyy}\right) + D_4\left(w^1_{,xx} + w^1_{,yy} + \psi^1_{x,x} + \psi^1_{y,y}\right) +$$

$$D_5\left(\phi_{,xx} + \phi_{,yy}\right) + N^0_{xx}w^1_{,xx} + 2N^0_{xy}w^1_{,xy} + N^0_{yy}w^1_{,yy} = 0$$

$$F_1\left(w^1_{,xxxx} + 2w^1_{,xxyy} + w^1_{,yyyy}\right) + F_2\left(\psi^1_{x,xxx} + \psi^1_{x,xyy} + \psi^1_{y,yxx} + \psi^1_{y,yyy}\right) +$$

$$F_3\left(u^1_{,xxx} + u^1_{,xyy} + v^1_{,yxx} + v^1_{,yyy}\right) + F_4\left(w^1_{,xx} + w^1_{,yy}\right) + F_5\left(\psi^1_{x,x} + \psi^1_{y,y}\right) + \tag{13}$$

$$F_6\left(u^1_{,x} + v^1_{,y}\right) + F_7\phi + F_8\left(\phi_{,xx} + \phi_{,yy}\right) = 0$$

where A_i, B_i, D_i and F_i (i=1 to 9) are introduced in the Appendices A and B for open and closed circuit conditions, respectively. Eq. (13) is six highly coupled partial differential equations in terms of neighboring displacement components and mid-plane electrical potential function.

4. Buckling analysis

In this study, a rectangular plate with length a and width b subjected to in-plane loads is considered as shown in Fig. 1. The pre-buckling forces can be obtained using the equilibrium conditions as

$$N^0_{xx} = -P_1, \quad N^0_{yy} = -P_2, \quad N^0_{xy} = 0 \tag{14}$$

where P_1 and P_2=RP_1 are the forces per unit length and R is the load ratio. With this definition, uniaxial loading in x-direction and baiaxial compressive loading in the x and y-directions are determined by R=0 and R=1, respectively while and R=−0 presents a plate under compressive in the x-direction and tensile loading in the y-direction.

The electrical and mechanical boundary conditions for a simply supported rectangular plate which its edges are covered with electrodes and electrically is under zero applied electric field (grounded to zero potential), can be expressed as follows
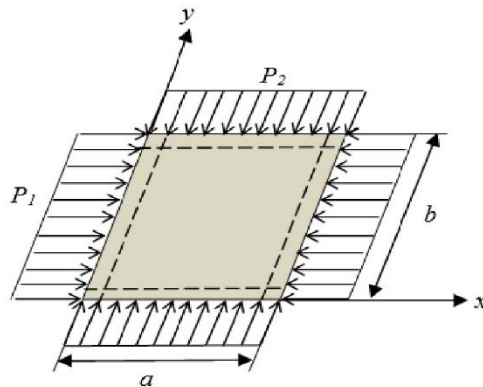

Fig. 1 Full simply supported rectangular plate subjected to the in-plane loads.

$$\phi = v^1 = w^1 = \psi_y^1 = M_{xx}^1 = P_{xx}^1 = 0 \qquad \text{at} \quad x = 0, a$$

$$\phi = u^1 = w^1 = \psi_x^1 = M_{yy}^1 = P_{yy}^1 = 0 \qquad \text{at} \quad y = 0, b \tag{15}$$

The differential Eq. (13) and boundary conditions (15) for simply-supported rectangular FGPM plate may be satisfied by double trigonometric expansions of the following forms

$$u(x, y) = \sum_{q=1}^{\infty} \sum_{p=1}^{\infty} \bar{U} \cos(\eta x) \sin(\mu y)$$

$$v(x, y) = \sum_{q=1}^{\infty} \sum_{p=1}^{\infty} \bar{V} \sin(\eta x) \cos(\mu y)$$

$$\psi_x(x, y) = \sum_{q=1}^{\infty} \sum_{p=1}^{\infty} \bar{\Psi}_x \cos(\eta x) \sin(\mu y)$$

$$\psi_y(x, y) = \sum_{q=1}^{\infty} \sum_{p=1}^{\infty} \bar{\Psi}_y \sin(\eta x) \cos(\mu y)$$

$$w(x, y) = \sum_{q=1}^{\infty} \sum_{p=1}^{\infty} \bar{W} \sin(\eta x) \sin(\mu y)$$

$$\phi(x, y) = \sum_{q=1}^{\infty} \sum_{p=1}^{\infty} \bar{\Phi} \sin(\eta x) \sin(\mu y) \tag{16}$$

Where $\mu = \pi q / b$ and $\eta = \pi p / a$ and p and q are the integer number of half-waves in the x and y directions of buckling mode shape, respectively. Substituting Eqs. (16) into (13), provides a set of homogenous algebraic equations in terms of coefficients and pre-buckling load P_1 which may be condensed in the following form

$$\begin{bmatrix} k_{11} & k_{12} & k_{13} & k_{14} & k_{15} & k_{16} \\ k_{21} & k_{22} & k_{23} & k_{24} & k_{25} & k_{26} \\ k_{31} & k_{32} & k_{33} & k_{34} & k_{35} & k_{36} \\ k_{41} & k_{42} & k_{43} & k_{44} & k_{45} & k_{46} \\ k_{51} & k_{52} & k_{53} & k_{54} & k_{55} & k_{56} \\ k_{61} & k_{62} & k_{63} & k_{64} & k_{65} & k_{66} \end{bmatrix} \begin{Bmatrix} \bar{\Phi} \\ \bar{\Psi}_x \\ \bar{\Psi}_y \\ \bar{U} \\ \bar{V} \\ \bar{W} \end{Bmatrix} = \begin{Bmatrix} 0 \\ 0 \\ 0 \\ 0 \\ 0 \\ 0 \end{Bmatrix} \tag{17}$$

Where k_{ij} (i,j=1 to 6)   are introduced in the Appendix C. Non-trivial solution of the system may be obtained when the determinant of the sixth order coefficient matrix is set equal to zero for the buckling loads which results the characteristic equation. To evaluate the buckling load of FGP plate the characteristic equation has to be solved. The critical buckling load is the minimum value among all these P_1 and denoted by P_{cr}.

5. Verification of results

In order to validate the accuracy of the present formulations, a comparison has been made with the previously published results. The first comparison carried out with the buckling analysis of FGM plates. For this purpose, aluminum (*E*=70 GPa) and silicon carbide (*E*=380 GPa) considered as bottom and top surface materials. Furthermore, the components of electric and dielectric matrix of piezoelectric material set equal to zero and elastic matrix components set equal to following

$$\overline{C}_{11} = \frac{E(z)}{1-v^2}, \quad \overline{C}_{22} = \frac{vE(z)}{1-v^2}, \quad \overline{C}_{22} = \frac{E(z)}{2(1+v)} \tag{18}$$

where *E*(*z*) is Young modulus that follow from Eq. (1). These considerations lead to FGPM

Table 1 Comparison of the critical buckling loads for a functionally graded plate with (2010b)

n	*R*	*a/b*	*h/b*					
			0.1			0.2		
			(2010b)	Closed	Open	(2010b)	Closed	Open
0	0	0.5	2079.721[1]	2079.758[1]	2079.758[1]	12162.119[1]	12164.991[1]	12164.991[1]
		1	1437.361[1]	1437.390[1]	1437.390[1]	9915.620[1]	9916.193[1]	9916.193[1]
		1.5	1527.903[2]	1527.994[2]	1527.994[2]	10044.721[2]	10044.962[2]	10044.962[2]
	1	0.5	1663.777[1]	1663.807[1]	1663.807[1]	9729.999[1]	9731.990[1]	9731.990[1]
		1	718.692[1]	718.695[1]	718.695[1]	4957.888[1]	4958.097[1]	4958.097[1]
		1.5	526.861[1]	526.862[1]	526.862[1]	3772.877[1]	3772.964[1]	3772.964[1]
	-1	0.5	2772.980[1]	2773.011[1]	2773.011[1]	16216.712[1]	16219.981[1]	16219.981[1]
		1	2772.980[2]	2773.011[2]	2773.011[2]	16216.712[2]	16219.981[2]	16219.981[2]
		1.5	2772.980[3]	2773.011[3]	2773.011[3]	16216.712[3]	16219.981[3]	16219.981[3]
1	0	0.5	1028.412[1]	1028.449[1]	1028.449[1]	6270.298[1]	6272.425[1]	6272.425[1]
		1	702.304[1]	702.251[1]	702.251[1]	4955.431[1]	4955.484[1]	4955.484[1]
		1.5	748.920[2]	748.988[2]	748.988[2]	5067.219[2]	5068.084[2]	5068.084[2]
	1	0.5	822.738[1]	822.759[1]	822.759[1]	5016.384[1]	5017.940[1]	5017.940[1]
		1	351.124[1]	351.126[1]	351.126[1]	2477.589[1]	2477.742[1]	2477.742[1]
		1.5	256.776[1]	256.776[1]	256.776[1]	1871.038[1]	1871.101[1]	1871.101[1]
	-1	0.5	1371.653[1]	1371.265[1]	1371.265[1]	8360.541[1]	8363.233[1]	8363.233[1]
		1	1371.653[2]	1371.265[2]	1371.265[2]	8360.541[2]	8363.233[2]	8363.233[2]
		1.5	1371.653[3]	1371.265[3]	1371.265[3]	8360.541[3]	8363.233[3]	8363.233[3]
2	0	0.5	780.097[1]	780.228[1]	780.228[1]	4692.542[1]	4695.029[1]	4695.029[1]
		1	534.441[1]	534.835[1]	534.835[1]	3746.054[1]	3746.732[1]	3746.732[1]
		1.5	569.751[2]	569.825[2]	569.825[2]	3819.109[2]	3820.079[2]	3820.079[2]
	1	0.5	624.158[1]	624.182[1]	624.182[1]	3754.274[1]	3756.023[1]	3756.023[1]
		1	267.416[1]	267.418[1]	267.418[1]	1873.190[1]	1873.366[1]	1873.366[1]
		1.5	195.714[1]	195.715[1]	195.715[1]	1418.120[1]	1418.193[1]	1418.193[1]
	-1	0.5	1040.519[1]	1040.304[1]	1040.304[1]	6257.811[1]	6260.038[1]	6260.038[1]
		1	1040.519[2]	1040.304[2]	1040.304[2]	6257.811[2]	6260.038[2]	6260.038[2]
		1.5	1040.519[3]	1040.304[3]	1040.304[3]	6257.811[3]	6260.038[3]	6260.038[3]

Table 2 Comparison of the critical buckling loads for a functionally graded piezoelectric plate with Ref. (2015) for open and closed circuit boundary conditions

a/b	h/b		Closed circuit condition			Open circuit condition		
			$R=1$	$R=0$	$R=-1$	$R=1$	$R=0$	$R=-1$
0.5	0.1	(2015)	**2.73338**	**3.41669**	**4.55561**	**2.77165**	**3.46453**	**4.61935**
		present	2.77848	3.47310	4.63081	2.81912	3.52390	4.69854
	0.2	(2015)	**1.95581**	**2.44476**	**3.25968**	**2.01841**	**2.52301**	**3.36402**
		Present	2.05334	2.56668	3.42222	2.13065	2.66331	3.55109
1	0.1	(2015)	**1.19144**	**2.38288**	**4.55561**	**1.20086**	**2.40165**	**4.61935**
		Present	1.20009	2.40018	4.63081	1.20968	2.41937	4.69854
	0.2	(2015)	**1.01122**	**2.02242**	**3.25968**	**1.03073**	**2.06147**	**3.36402**
		Present	1.03608	2.07215	3.42222	1.05756	2.11512	3.55109
1.5	0.1	(2015)	**0.87518**	**2.52655**	**4.55561**	**0.88101**	**2.55058**	**4.61935**
		Present	0.87987	2.55124	4.63081	0.88581	2.57608	4.69854
	0.2	(2015)	**0.77327**	**2.03767**	**3.25968**	**0.78524**	**2.08622**	**3.36402**
		Present	0.78774	2.10295	3.42222	0.80056	2.15821	3.55109

Table 3 Material properties of some common piezoelectric materials

Materials	Elastic constants (GPa)					Electric constants (C/m²)			Dielectric constants (C/Vm)	
	C_{11}^E	C_{33}^E	C_{55}^E	C_{12}^E	C_{13}^E	e_{33}	$-e_{13}$	e_{15}	Ξ_{11}	Ξ_{33}
PZT-4	132	115	26	71	73	14.1	4.1	10.5	7.124e-9	5.841 e-9
PZT-5A	121	111	21.1	75.9	75.4	15.8	5.4	12.3	8.11 e-9	7.35 e-9
PZT-6B	168	163	35.5	84.7	84.2	7.10	0.9	4.60	3.60 e-9	3.42 e-9
PZT-5H	126	117	23.0	79.1	83.9	23.3	6.5	17.0	15.1 e-9	13.0 e-9
PZT-7A	148	131	25.3	76.1	81.3	9.50	2.1	9.20	4.07 e-9	2.08 e-9
PZT-8	137	123	31.3	69.9	71.1	17.5	4.0	10.4	7.97 e-9	5.14 e-9
PIC-151	107.6	100.4	19.6	63.1	63.9	15.14	9.52	11.97	9.837 e-9	8.190 e-9
PZT(NEPEC6)	139	115	25.6	77.8	74.3	15.1	5.2	12.7	6.463 e-9	5.622 e-9
BaTiO₃	166	162	43	77	78	18.6	4.4	11.6	11.2 e-9	12.6 e-9

becomes FGM and comparable with (2010b). As it can be seen from the Table 1, the results obtained using this method coincides with the previous results (2010b) and therefore its merits and accuracy are verified. Other comparison has been made with (2015). For this purpose, PZT-4 and PZT-5H considered as bottom and top surface materials, respectively. From results shown in Table 2, it can be seen that accuracy of this method is verified.

6. Results and discussion

In order to present the following new results, it is assumed that the FGP plate is made of a mixture of BaTiO3 and PZT-7A as the bottom and top surfaces of the plate, respectively. The

Table 4 The critical buckling load of a functionally graded plate for various electrical conditions

| n | R | h/b | a/b |
| | | | 0.5 | 1.0 | 1.5 | 0.5 | 1.0 | 1.5 | 0.5 | 1.0 | 1.5 |
			\multicolumn{3}{c}{Closed}	\multicolumn{3}{c}{Open}	\multicolumn{3}{c}{Without piezoelectric effect}
0	0	0.1	538.2492	373.8301	396.7853	555.4326	379.4843	404.7503	421.4200	298.2318	314.9580
		0.2	3143.443	2559.500	2589.840	3345.881	2671.422	2725.276	2286.695	1969.789	1960.785
	1	0.1	430.5993	186.9151	137.1919	444.3461	189.7421	138.7410	337.1360	149.1159	109.8496
		0.2	2514.755	1279.750	975.6022	2676.704	1335.711	1010.131	1829.356	984.8945	760.3378
	-1	0.1	717.6655	717.6655	717.6655	740.5768	740.5768	740.5768	561.8933	561.8933	561.8933
		0.2	4191.258	4191.258	4191.258	4461.174	4461.174	4461.174	3048.926	3048.926	3048.926
1	0	0.1	559.5527	388.0333	412.0753	592.6676	408.5036	434.5867	496.7678	346.9205	367.7324
		0.2	3261.033	2662.141	2693.231	3494.909	2831.985	2874.175	2808.771	2347.729	2359.595
	1	0.1	447.6421	194.0167	142.3422	474.1340	204.2518	149.6460	397.4143	173.4602	127.4315
		0.2	2608.826	1331.071	1014.430	2795.927	1415.993	1075.833	2247.017	1173.864	899.0207
	-1	0.1	746.0702	746.0702	746.0702	790.2234	790.2234	790.2234	662.3571	662.3571	662.3571
		0.2	4348.043	4348.043	4348.043	4659.878	4659.878	4659.878	3745.028	3745.028	3745.028
2	0	0.1	581.6098	401.3359	426.7912	612.8203	421.7752	448.8709	515.6971	358.1183	380.1927
		0.2	3440.002	2778.398	2820.729	3637.017	2932.617	2980.616	2969.308	2448.826	2471.614
	1	0.1	465.2879	200.6679	147.0701	490.2563	210.8876	154.4687	412.5577	179.0591	131.3927
		0.2	2752.001	1389.199	1055.614	2909.614	1466.308	1112.847	2375.446	1224.413	934.5010
	-1	0.1	775.4798	775.4798	775.4798	817.0938	817.0938	817.0938	687.5962	687.5962	687.5962
		0.2	4586.669	4586.669	4586.669	4849.356	4849.356	4849.356	3959.077	3959.077	3959.077

Poisson ratio of the plate is assumed to be constant through the thickness and equal to 0.3. The material properties of various piezoelectric materials are listed in Table 3.

Table 4 shows a comparison between the critical buckling loads of open, closed and "without piezoelectric effect" conditions. For "without piezoelectric effect" condition, the reduced matrix of piezoelectric constants $[e]$ and the dielectric constants matrix $[\Xi]$ are considered to be zero. In this condition only stiffness of FGP plate is considered. In this Table, the critical buckling loads have been tabulated for the FGP plate under three loading conditions, some material power law indices and different thickness-side (h/b) and different aspect ratios (a/b). From the results presented in the Table, it is concluded that the "without piezoelectric effect" condition has the critical buckling loads less than closed and open circuit conditions.

That means the piezoelectric effect leads to increase the critical buckling load. Moreover, for all mentioned loading conditions, the critical buckling load increased as thickness-side ratio increased. Furthermore, increasing in thickness-side ratio leads to increase the number of half-waves in the critical buckling mode shape.

In Fig. 2 the critical buckling load for FGP plate has been shown versus the electrical boundary conditions. The plate is subjected to biaxial compression and tension along x and y directions, respectively. It is seen that the critical buckling load of open circuit condition is higher than that of closed and "without piezoelectric effect" condition. Therefore, by changing electrical boundary condition from closed to open circuit condition, one can easily change the critical

Table 5 Various case studies for investigation of piezoelectric material constants effect

Case No.	Elastic constants	Piezoelectric constants	Dielectric constants
1	Changed	Fixed	Fixed
2	Fixed	Changed	Fixed
3	Fixed	Fixed	Changed
4	Changed	Changed	Fixed
5	Changed	Fixed	Changed
6	Fixed	Changed	Changed
7	Changed	Changed	Changed
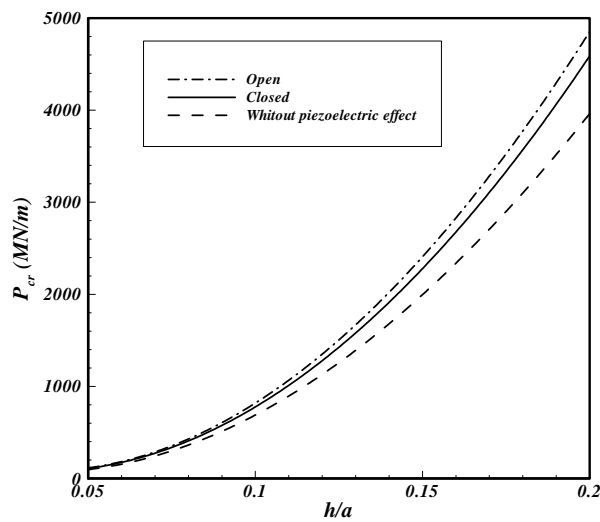
Fig. 2 The critical buckling load for an FGP plate (*a/b*=0.5, *n*=2, *R*=−1)
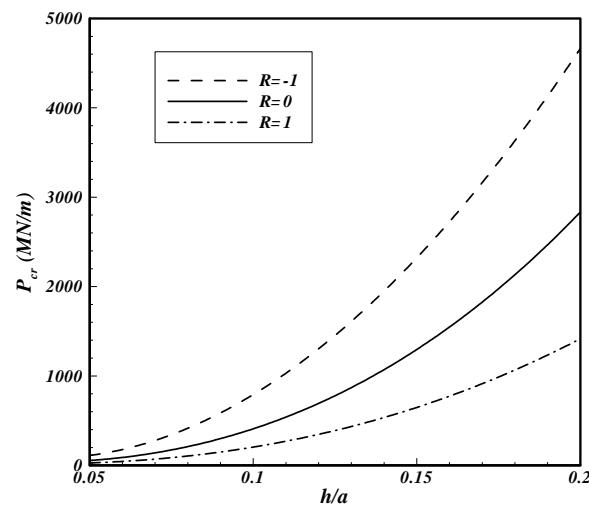
Fig. 3 The critical buckling loads of an FGP plate versus the thickness to side ratio under different kinds of loading conditions for open circuit condition (*a/b*=1, *n*=1)
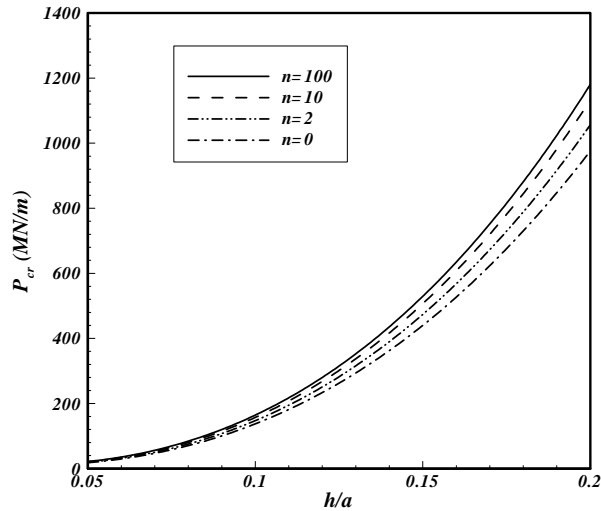
Fig. 4 The critical buckling loads of an FGP plate versus the thickness to side ratio subjected to biaxial compression with some material power law indices for closed circuit condition (*a/b*=1.5)
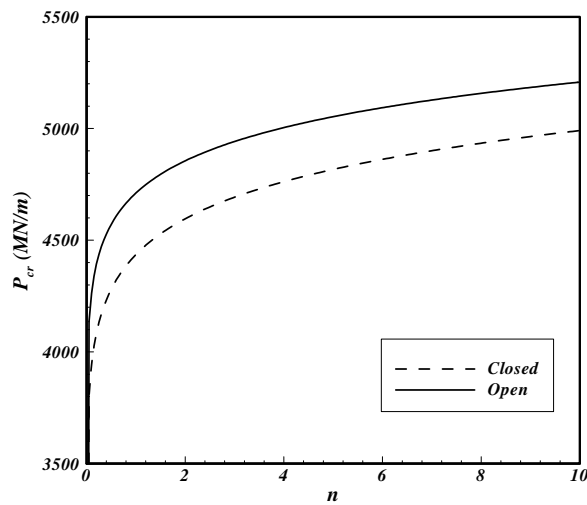
Fig. 5 The critical buckling load of an FGP plate versus material power law index for open and closed circuit conditions (*a/b*=0.5, *h/b*=0.2, *R*=−1)

buckling load without altering material properties. In the vibration absorbing and harvest energy from vibrating structures, this phenomenon is known as piezoelectric shunting (2009b). Besides, the critical buckling load and difference between the critical buckling load of closed and open circuit condition increases as the thickness to side ratio increases i.e., the growth rate of the critical buckling load of open circuit condition is more than that of closed circuit condition.

Fig. 3 shows the critical buckling loads of an FGP plate versus the thickness to side ratio under different kinds of loading conditions for open circuit condition. It can be seen that the highest and lowest values of the critical buckling load are related to biaxial compression and tension (*R*=−1)
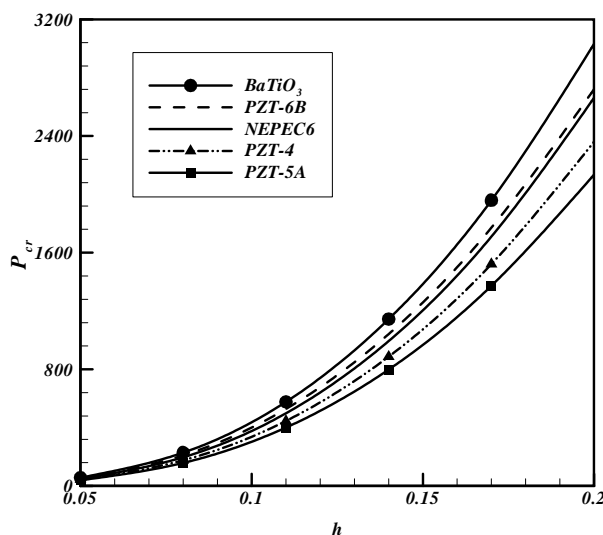
Fig. 6 The critical buckling load of different piezoelectric materials for open circuit condition under biaxial compression loading (*a/b*=1, *n*=0)

and biaxial compression (*R*=1), respectively. The critical buckling loads of an FGP plate versus the thickness to side ratio subjected to biaxial compression with some material power law indices for closed circuit condition depicted in Fig. 4. It is observed that the critical buckling load increases with the increase of material power law indices.

Fig. 5 presents the critical buckling load of an FGP plate subjected to biaxial compression and tension loading versus material power law index for open and closed circuit conditions. As shown before, increasing of the material power law index leads to increase of the critical buckling load. Moreover, in smaller material power law indices the change of the critical buckling load is more obvious for both open and closed circuit conditions.

The critical buckling load of different piezoelectric materials for open circuit condition under biaxial compression loading is shown in Fig. 6. For this purpose, the material power law index of FGP is set to zero to make it a homogeneous material. Furthermore, material properties of the top ($z=h/2$) surfaces of the plate is changed to every specified piezoelectric material. As the figure shows, the least and the most values of critical buckling loads are related to PZT-5A and BaTio$_3$, respectively.

To investigate the effect of the difference between the top and bottom piezoelectric material, the parameter δ which varies between zero and one is introduced. The material properties of the bottom surface of plate varies from PZT-7A to BaTio3 as δ varies from zero to one, wheras the material properties of the top surface plate are fixed at BaTio3. Fig. 7 shows the critical buckling load of FGP plate versus δ for both open and closed condiotions. It is seen that the critical buckling load increases as δ increases that means the critical buckling load of pure BaTio3 plate is greater than FGP plate that made of PZT-7A and BaTio3. Moreover, difference between the critical buckling load of open and closed circuit condition decreases as δ increases.

Some other studied cases are shown in Table 5. In this table "changed" means that related variables varies as δ varies i.e., $\Theta(z)$ changes to $\delta\Theta(z)$ where δ varies as before. Cases Nos. 1, 2 and 3 are related to variation in elastic, piezoelectric and dielectric constants of FGP plate,
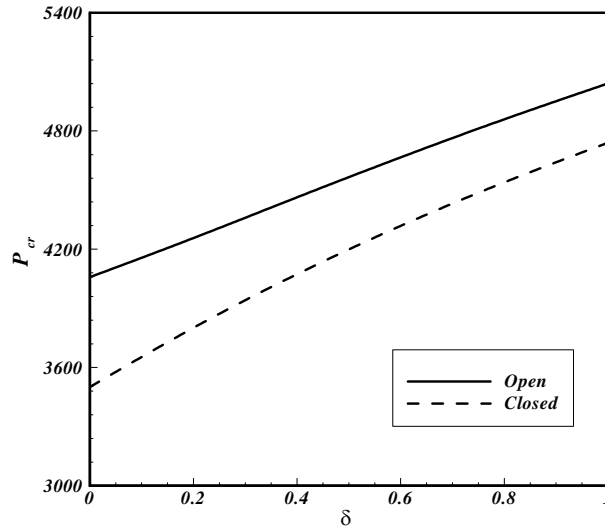
Fig. 7 The critical buckling load of an FGP plate versus δ for open and closed conditions (a/b=0.5, h/b=0.2, R=−1, n=2)
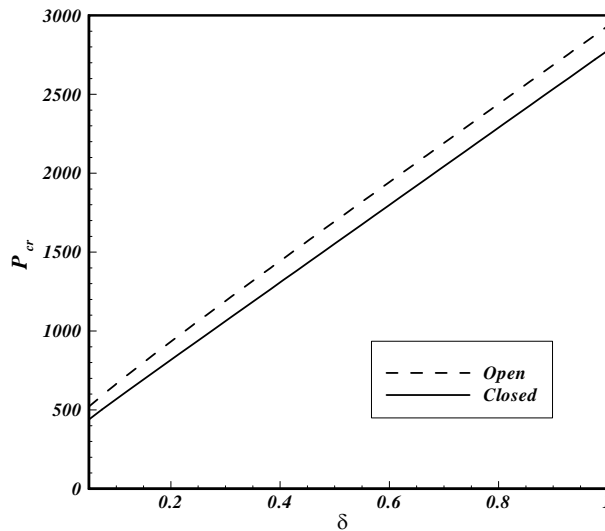

Fig. 8 The critical buckling load of an FGP plate versus δ for case No. 1 under open and closed circuit conditions (a/b=1, h/b=0.2, R=0)

respectively. In cases Nos. 4 to 6 two sets of constants vary and in the case No. 7 all constants vary. In the Figs. 8 to 14 the critical buckling loads of FGP plates versus δ for various cases under open and closed circuit conditions at R=0 are presented. It is observed that the critical buckling load of case No. 1 is increased linearly when δ increases, Fig. 8.

In order to explain this phenomenon, the scalar version of piezoelectric constitutive relationships is referred as follows (2009b)

$$\sigma = C\varepsilon - eE, \tag{19a}$$

$$D = e\varepsilon + \Xi E. \tag{19b}$$

Substituting (19b) into (19a) gives

$$\sigma = \left(C + \frac{e^2}{\Xi}\right)\varepsilon - \frac{e}{\Xi}D \tag{20}$$

For open circuit condition, electric displacement field is zero, hence Eq. (20) is reduced to

$$\sigma = \left(C + \frac{e^2}{\Xi}\right)\varepsilon \tag{21}$$

Introducing $C + \dfrac{e^2}{\Xi}$ as equivalent stiffness of open circuit condition, it can be seen that by increasing C stress increases linearly. Similarly in the case No. 2 by increasing δ, the critical buckling load increases quadratic, Fig. 9.

Moreover, the critical buckling load decreases as hyperbolic function due to the existence of dielectric constant in the denominator, Fig. 10. Comparing Figs. 8 to 10 and considering the variation range of the critical buckling load (vertical axis), it may be concluded that the effect of dielectric constants variation on the critical buckling load is more than that of two others.

In Fig. 11, piezoelectric and elastic constants are increased simultaneously. According to greater values of elastic constants, these constants have a dominant effect on critical buckling load. Thus, the variation of critical buckling load versus δ has linear behavior instead of quadratic ones. Refer to Fig. 12 it is concluded that, in the lower values of δ, the effect of dielectric constants is dominant thus the critical buckling load behaves as hyperbolic whereas in the higher values of δ,
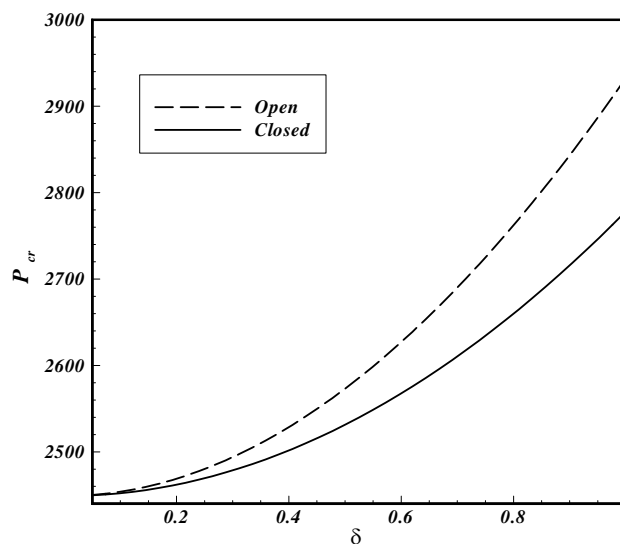

Fig. 9 The critical buckling load of an FGP plate versus δ for case No. 2 under open and closed circuit conditions (a/b=1, h/b=0.2, R=0)
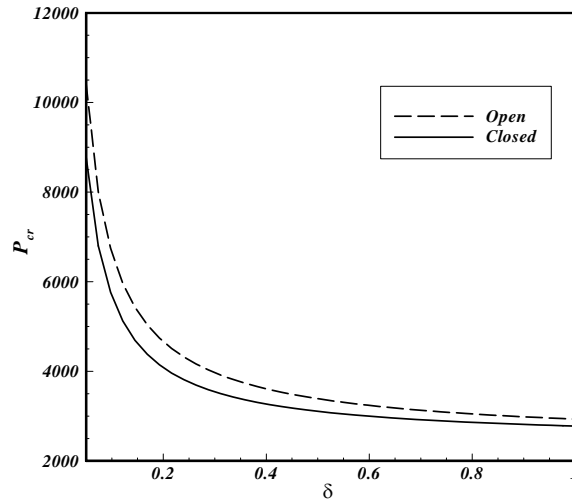
Fig. 10 The critical buckling load of an FGP plate versus δ for case No. 3 under open and closed circuit condition (a/b=1, h/b=0.2, R=0)
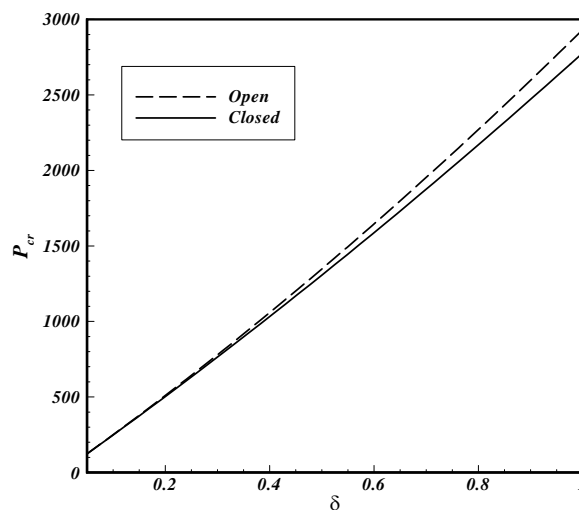

Fig. 11 The critical buckling load of an FGP plate versus δ for case No. 4 under open and closed circuit conditions (a/b=1, h/b=0.2, R=0)

dominant effect of elastic constants leads to linear behavior of critical buckling load.

In the case No. 6, the critical buckling load increases as δ increases, Fig. 13. It seems that the piezoelectric constants are more effective than dielectric ones on the critical buckling load.

The effects of all constants on the critical buckling load are studied in Fig. 14. Due to the linear behavior of diagram, it is found that the elastic constants have a dominant effect on the critical buckling load in this case. Furthermore, according to Figs. 9, 11, 13 and 14, in lower values of δ the critical buckling load of open and closed circuit conditions are the same because of weak coupling between the mechanical and electrical fields due to lower values of piezoelectric constants.
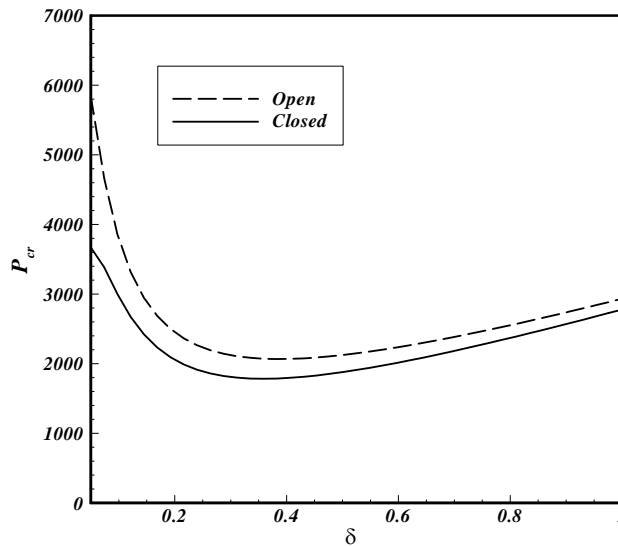
Fig. 12 The critical buckling load of an FGP plate versus δ for case No. 5 under open and closed circuit conditions (a/b=1, h/b=0.2, R=0)
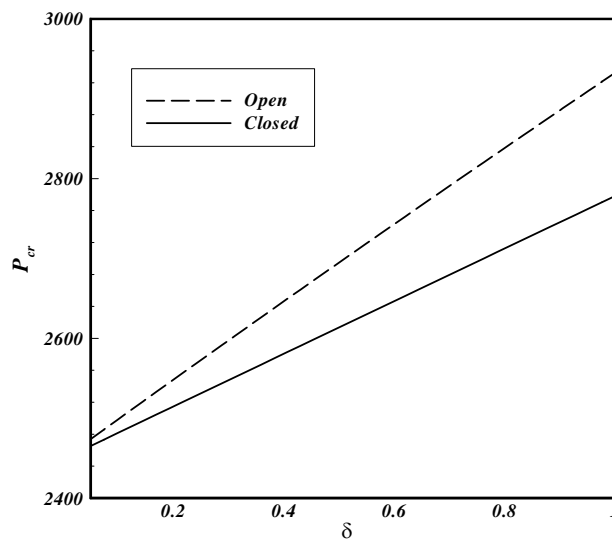

Fig. 13 The critical buckling load of an FGP plate versus δ for case No. 6 under open and closed circuit conditions (a/b=1, h/b=0.2, R=0)

In Fig. 15 the critical buckling load for an FGP plate has been plotted versus the aspect ratio of plate for electrical boundary conditions. The plate is subjected to uniaxial compression. It can be seen that the critical buckling load decreases by increasing the aspect ratio for all electrical boundary conditions. Moreover, the critical buckling load of closed circuit condition is less than that of open circuit condition and greater than "without piezoelectric effect" condition. Moreover, it can be observed that by increasing the aspect ratio the critical mode number of buckling is increased. According to these results, it can be concluded that the piezoelectric phenomenon has
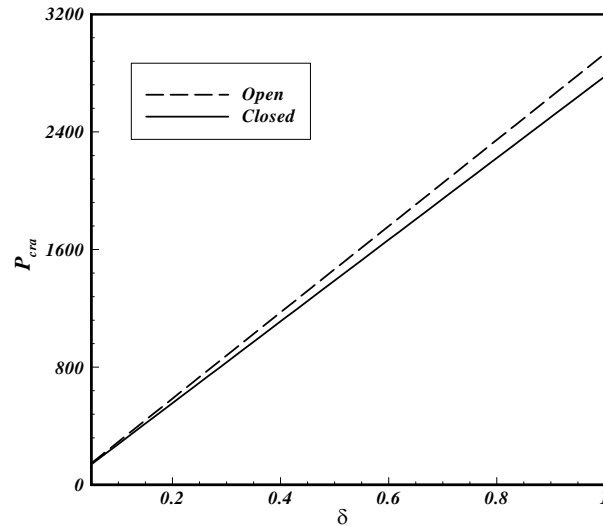
Fig. 14 The critical buckling load of an FGP plate versus δ for case No. 7 under open and closed circuit conditions (a/b=1, h/b=0.2, R=0)
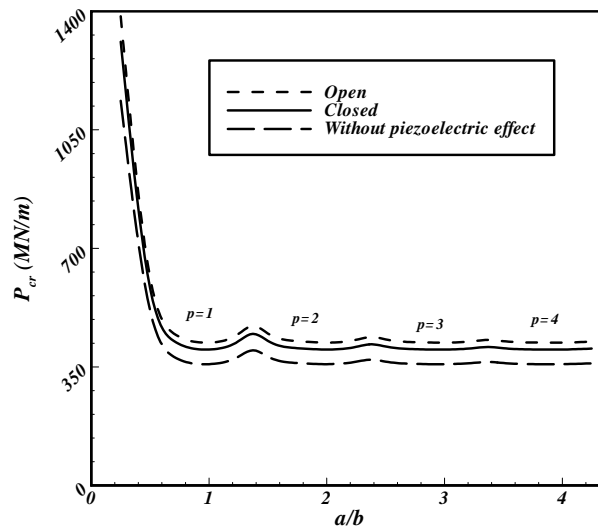
Fig. 15 The critical buckling load of an FGP plate versus the aspect ratio under uniaxial compression (h/b=0.1, n=0)

no effect on the critical mode number of buckling.

7. Conclusions

In the present article, an analytical method was developed for buckling analysis of FGP rectangular plates. Based on the higher-order shear deformation plate theory, the stability and

equilibrium equations were derived. Six coupled stability equations were solved using double sine series solution. The critical buckling loads for fully simply-supported boundary condition and closed and open circuit electrical boundary conditions were presented. From the numerical results the following conclusions are emphasized:

    1. The electrical effect of FGPM increases the critical buckling load for both open and closed circuit conditions.

    2. The critical buckling load increases as the thickness of FGP plate increases for all electrical and loading conditions, the critical buckling load increases as the thickness of FGP plate increases.

    3. In all loading conditions, changing the open circuit condition to the closed one reduces the critical buckling loads.

    4. In all electrical boundary conditions, the highest and lowest values for the critical buckling load are related to the plates under biaxial compression, and tension and biaxial compression, respectively.

    5. The effect of variation in dielectric constants on the critical buckling load is more significant than that of other constants of FGPM.

    6. The piezoelectric phenomenon has no effect on the critical mode number of buckling.

References

Abdollahi, M., Saidi, A. and Mohammadi, M. (2015), "Buckling analysis of thick functionally graded piezoelectric plates based on the higher-order shear and normal deformable theory", *Acta Mechanica*, **226**(8), 1-14.

Akbarov, S.D. and Yahnioglu, N. (2013a), "Buckling delamination of a sandwich plate-strip with piezoelectric face and elastic core layers", *Appl. Math. Model.*, **37**(16), 8029-8038.

Akgöz, B. and Civalek, Ö. (2014a), "Thermo-mechanical buckling behavior of functionally graded microbeams embedded in elastic medium", *Int. J. Eng. Sci.*, **85**, 90-104.

Akhras, G. and Li, W. (2010a), "Three-dimensional thermal buckling analysis of piezoelectric antisymmetric angle-ply laminates using finite layer method", *Compos. Struct.*, **92**(1), 31-38.

Batra, R. and Geng, T. (2001a), "Enhancement of the dynamic buckling load for a plate by using piezoceramic actuators", *Smart Mater. Struct.*, **10**(5), 925-933.

Bodaghi, M. and Saidi, A. (2010b), "Levy-type solution for buckling analysis of thick functionally graded rectangular plates based on the higher-order shear deformation plate theory", *Appl. Math. Model.*, **34**(11), 3659-3673.

Brush, D.O. and Almroth, B. (1979), *Buckling of Bars, Plates, and Shells*, McGraw-Hill, New York.

Chandrashekhara, K. and Bhatia, K. (1993), "Active buckling control of smart composite plates-finite-element analysis", *Smart Mater. Struct.*, **2**(1), 31-39.

Civalek, Ö. (2004a), "Application of differential quadrature (DQ) and harmonic differential quadrature (HDQ) for buckling analysis of thin isotropic plates and elastic columns", *Eng. Struct.*, **26**(2), 171-186.

Civalek, Ö., Korkmaz, A. and Demir, Ç. (2010c), "Discrete singular convolution approach for buckling analysis of rectangular Kirchhoff plates subjected to compressive loads on two-opposite edges", *Adv. Eng. Softw.*, **41**(4), 557-560.

Ebrahimi, F., Rastgoo, A. and Atai, A. (2009a), "A theoretical analysis of smart moderately thick shear deformable annular functionally graded plate", *Euro. J. Mech. A/Solid.*, **28**(5), 962-973.

Fereidoon, A., Yaghoobi, H. and Dehghanian, A. (2014b), "An analytical approach for buckling behavior of temperature-dependent laminated piezoelectric functionally graded plates under thermo-electro-mechanical loadings and different end supports", *Int. J. Comput. Meth.*, **11**(04), 1350099.

Hosseini-Hashemi, S., Khorshidi, K. and Amabili, M. (2008a), "Exact solution for linear buckling of rectangular Mindlin plates", *J. Sound Vib.*, **315**(1), 318-342.

Jadhav, P. and Bajoria, K. (2013b), "Stability analysis of piezoelectric FGM plate subjected to electro-mechanical loading using finite element method", *Int. J. Appl. Sci. Eng.*, **11**(4), 375-391.

Jalili, N. (2009b), *Piezoelectric-based vibration control: from macro to micro/nano scale systems*, Springer Science & Business Media.

Javaheri, R. and Eslami, M. (2002a), "Thermal buckling of functionally graded plates", *AIAA J.*, **40**(1), 162-169.

Javaheri, R. and Eslami, M. (2002b), "Thermal buckling of functionally graded plates based on higher order theory", *J. Therm. Stress.*, **25**(7), 603-625.

Jones, R.M. (2006a), *Buckling of bars, plates, and shells*, Bull Ridge Corporation.

Kapuria, S. and Achary, G. (2006b), "Nonlinear coupled zigzag theory for buckling of hybrid piezoelectric plates", *Compos. Struct.*, **74**(3), 253-264.

Kim, G.W. and Lee, K.Y. (2008b), "Influence of weak interfaces on buckling of orthotropic piezoelectric rectangular laminates", *Compos. Struct.*, **82**(2), 290-294.

Kim, S.E., Thai, H.T. and Lee, J. (2009c), "Buckling analysis of plates using the two variable refined plate theory", *Thin Wall. Struct.*, **47**(4), 455-462.

Kuo, S.R. and Yau, J. (2012), "Buckling equations of orthotropic thin plates", *J. Mech.*, **28**(03), 555-567.

Lanhe, W. (2004b), "Thermal buckling of a simply supported moderately thick rectangular FGM plate", *Compos. Struct.*, **64**(2), 211-218.

Mirzavand, B. and Eslami, M. (2011a), "A closed-form solution for thermal buckling of piezoelectric FGM rectangular plates with temperature-dependent properties", *Acta Mechanica*, **218**(1-2), 87-101.

Mohammadi, M., Saidi, A. and Jomehzadeh, E. (2010d), "A novel analytical approach for the buckling analysis of moderately thick functionally graded rectangular plates with two simply-supported opposite edges", *Proceedings of the Institution of Mechanical Engineers, Part C: Journal of Mechanical Engineering Science*, **224**(9), 1831-1841.

Mohammadi, M., Saidi, A.R. and Jomehzadeh, E. (2010e), "Levy solution for buckling analysis of functionally graded rectangular plates", *Appl. Compos. Mater.*, **17**(2), 81-93.

Panahandeh-Shahraki, D., Mirdamadi, H.R. and Vaseghi, O. (2014c), "Fully coupled electromechanical buckling analysis of active laminated composite plates considering stored voltage in actuators", *Compos. Struct.*, **118**, 94-105.

Rad, A.A. and Panahandeh-Shahraki, D. (2014d), "Buckling of cracked functionally graded plates under tension", *Thin Wall. Struct.*, **84**, 26-33.

Shariat, B.S. and Eslami, M. (2007), "Buckling of thick functionally graded plates under mechanical and thermal loads", *Compos. Struct.*, **78**(3), 433-439.

Shariyat, M. (2009d), "Dynamic buckling of imperfect laminated plates with piezoelectric sensors and actuators subjected to thermo-electro-mechanical loadings, considering the temperature-dependency of the material properties", *Compos. Struct.*, **88**(2), 228-239.

Shariyat, M. (2009e), "Vibration and dynamic buckling control of imperfect hybrid FGM plates with temperature-dependent material properties subjected to thermo-electro-mechanical loading conditions", *Compos. Struct.*, **88**(2), 240-252.

Shen, H.S. (2001b), "Postbuckling of shear deformable laminated plates with piezoelectric actuators under complex loading conditions", *Int. J. Solid. Struct.*, **38**(44), 7703-7721.

Shen, H.S. (2001c), "Thermal postbuckling of shear-deformable laminated plates with piezoelectric actuators", *Compos. Sci. Tech.*, **61**(13), 1931-1943.

Shen, H.S. (2005), "Postbuckling of FGM plates with piezoelectric actuators under thermo-electro-mechanical loadings", *Int. J. Solid. Struct.*, **42**(23), 6101-6121.

Shen, H.S. (2009f), "A comparison of buckling and postbuckling behavior of FGM plates with piezoelectric fiber reinforced composite actuators", *Compos. Struct.*, **91**(3), 375-384.

Sheng, G. and Wang, X. (2010f), "Thermoelastic vibration and buckling analysis of functionally graded piezoelectric cylindrical shells", *Appl. Math. Model.*, **34**(9), 2630-2643.

Varelis, D. and Saravanos, D.A. (2004c), "Coupled buckling and postbuckling analysis of active laminated piezoelectric composite plates", *Int. J. Solid. Struct.*, **41**(5), 1519-1538.

Yang, Y. (1998), "Buckling of a piezoelectric plate", *Int. J. Appl. Electromag. Mech.*, **9**(40), 399-408.

Yoo, C.H. and Lee, S. (2011b), *Stability of structures: principles and applications*, Elsevier.

PL

Appendix A

Open circuit condition constants

$$A_1 = -\int_{-h/2}^{h/2}\left(\bar{C}_{11}^E(z)\alpha z^3 + \frac{\bar{e}_{31}(z)\bar{e}_{31b}\alpha h^3}{8\bar{\Xi}_{33b}}\right)dz \tag{A.1}$$

$$A_2 = -\int_{-h/2}^{h/2}\left(\bar{C}_{11}^E(z)(z-\alpha z^3) - \frac{\bar{e}_{31}(z)\bar{e}_{31b}h(1-\alpha h^2/4)}{2\bar{\Xi}_{33b}}\right)dz \tag{A.2}$$

$$A_3 = \frac{1}{2}\int_{-h/2}^{h/2}\left(\bar{C}_{11}^E(z) - \bar{C}_{12}^E(z)\right)(z-\alpha z^3)dz \tag{A.3}$$

$$A_4 = \frac{1}{2}\int_{-h/2}^{h/2}\left(\left(\bar{C}_{11}^E(z) + \bar{C}_{12}^E(z)\right)(z-\alpha z^3) + \frac{\bar{e}_{31}(z)\bar{e}_{31b}h(1-\alpha h^2/4)}{\bar{\Xi}_{33b}}\right)dz \tag{A.4}$$

$$A_5 = \int_{-h/2}^{h/2}\left(\bar{C}_{11}^E(z) + \frac{\bar{e}_{31}(z)\bar{e}_{31b}}{\bar{\Xi}_{33b}}\right)dz \tag{A.5}$$

$$A_6 = \frac{1}{2}\int_{-h/2}^{h/2}\left(\bar{C}_{11}^E(z) - \bar{C}_{12}^E(z)\right)dz \tag{A.6}$$

$$A_7 = \frac{1}{2}\int_{-h/2}^{h/2}\left(\bar{C}_{11}^E(z) + \bar{C}_{12}^E(z) + \frac{2\bar{e}_{31}(z)\bar{e}_{31b}}{\bar{\Xi}_{33b}}\right)dz \tag{A.7}$$

$$A_8 = \int_{-h/2}^{h/2}\frac{4\bar{e}_{31}(z)}{h}\left(1-\frac{2z}{h}\right)dz \tag{A.8}$$

$$B_1 = -\int_{-h/2}^{h/2}\left\{\left(\bar{C}_{11}^E(z)\alpha z^3 + \frac{\bar{e}_{31}(z)\bar{e}_{31b}\alpha h^3}{8\bar{\Xi}_{33b}}\right)(z-\alpha z^3) + \frac{\alpha\bar{e}_{15}(z)\bar{e}_{31b}h^3(z+h/2)(3\alpha z^2-1)}{8\bar{\Xi}_{33b}}\right\}dz \tag{A.9}$$

$$B_2 = \int_{-h/2}^{h/2}\left\{\left(\bar{C}_{11}^E(z)(z-\alpha z^3) + \frac{\bar{e}_{31}(z)\bar{e}_{31b}(1-\alpha h^2/4)h}{2\bar{\Xi}_{33b}}\right)(z-\alpha z^3) + \right.$$
$$\left. \frac{\bar{e}_{15}(z)\bar{e}_{31b}(z+h/2)(1-\alpha h^2/4)(3\alpha z^2-1)h}{2\bar{\Xi}_{33b}}\right\}dz \tag{A.10}$$

$$B_3 = \frac{1}{2}\int_{-h/2}^{h/2}\left(\bar{C}_{11}^E(z) - \bar{C}_{12}^E(z)\right)(z-\alpha z^3)^2\,dz \tag{A.11}$$

$$B_4 = \frac{1}{2} \int\limits_{-h/2}^{h/2} \left\{ \left(\left(\bar{C}_{11}^E(z) + \bar{C}_{12}^E(z) \right)\left(z - \alpha z^3 \right) + \frac{\bar{e}_{31}(z)\bar{e}_{31b}\left(1 - \alpha h^2/4 \right)h}{\bar{\bar{\Xi}}_{33b}} \right)\left(z - \alpha z^3 \right) + \right.$$
$$\left. \frac{\bar{e}_{15}(z)\bar{e}_{31b}\left(z + h/2 \right)\left(1 - \alpha h^2/4 \right)\left(3\alpha z^2 - 1 \right)h}{\bar{\bar{\Xi}}_{33b}} \right\} dz \tag{A.12}$$

$$B_5 = \int\limits_{-h/2}^{h/2} \left\{ \left(\bar{C}_{11}^E(z) + \frac{\bar{e}_{31}(z)\bar{e}_{31b}}{\bar{\bar{\Xi}}_{33b}} \right)\left(z - \alpha z^3 \right) + \frac{\bar{e}_{15}(z)\bar{e}_{31b}\left(z + h/2 \right)\left(3\alpha z^2 - 1 \right)}{\bar{\bar{\Xi}}_{33b}} \right\} dz \tag{A.13}$$

$$B_6 = \frac{1}{2} \int\limits_{-h/2}^{h/2} \left(\bar{C}_{11}^E(z) - \bar{C}_{12}^E(z) \right)\left(1 - \alpha z^3 \right) dz \tag{A.14}$$

$$B_7 = \frac{1}{2} \int\limits_{-h/2}^{h/2} \left\{ \left(\bar{C}_{11}^E(z) + \bar{C}_{12}^E(z) + \frac{2\bar{e}_{31}(z)\bar{e}_{31b}}{\bar{\bar{\Xi}}_{33b}} \right)\left(z - \alpha z^3 \right) + \right.$$
$$\left. \frac{\bar{e}_{15}(z)\bar{e}_{31b}\left(z + h/2 \right)\left(3\alpha z^2 - 1 \right)}{\bar{\bar{\Xi}}_{33b}} \right\} dz \tag{A.15}$$

$$B_8 = -\int\limits_{-h/2}^{h/2} C_{55}^E(z)\left(1 - 3\alpha z^2 \right)^2 dz \tag{A.16}$$

$$B_9 = \int\limits_{-h/2}^{h/2} \left\{ \left(\frac{4\bar{e}_{31}(z)}{h} \right)\left(1 - \frac{2z}{h} \right)\left(1 - \alpha z^3 \right) + \bar{e}_{15}(z)\left(\frac{4z^2}{h^2} - \frac{4z}{h} - 3 \right)\left(1 - \alpha z^3 \right) \right\} dz \tag{A.17}$$

$$D_1 = -\alpha \int\limits_{-h/2}^{h/2} \left\{ \left(\bar{C}_{11}^E(z)z^3 + \frac{\bar{e}_{31}(z)\bar{e}_{31b}h^3}{8\bar{\bar{\Xi}}_{33b}} \right)z^3 + \right.$$
$$\left. \frac{\bar{e}_{15}(z)\bar{e}_{31b}h^3\left(z + h/2 \right)\left(3\alpha z^2 - 1 \right)}{8\bar{\bar{\Xi}}_{33b}} \right\} dz \tag{A.18}$$

$$D_2 = \alpha \int\limits_{-h/2}^{h/2} \left\{ \frac{\bar{e}_{15}(z)\bar{e}_{31b}\left(z + h/2 \right)\left(1 - \alpha h^2/4 \right)\left(3\alpha z^2 - 1 \right)h}{2\bar{\bar{\Xi}}_{33b}} + \right.$$
$$\left. \left(\bar{C}_{11}^E(z)\left(z - \alpha z^3 \right) + \frac{\bar{e}_{31}(z)\bar{e}_{31b}\left(1 - \frac{\alpha h^2}{4} \right)h}{2\bar{\bar{\Xi}}_{33b}} \right)z^3 \right\} dz \tag{A.19}$$

$$D_3 = \alpha \int\limits_{-h/2}^{h/2} \left\{ \left(\bar{C}_{11}^E(z) + \frac{\bar{e}_{31}(z)\bar{e}_{31b}}{\bar{\bar{\Xi}}_{33b}} \right) z^3 + \frac{\bar{e}_{15}(z)\bar{e}_{31b}(z+h/2)(3\alpha z^2 - 1)}{\bar{\bar{\Xi}}_{33b}} \right\} dz \tag{A.20}$$

$$D_4 = -B_8 \tag{A.21}$$

$$D_5 = \alpha \int\limits_{-h/2}^{h/2} \left\{ \frac{4\bar{e}_{31}(z)}{h}(1-2z/h)z^3 + \bar{e}_{15}(z)\left(\frac{4z^2}{h^2} - \frac{4z}{h} - 3 \right)(3\alpha z^2 - 1) \right\} dz \tag{A.22}$$

$$F_1 = \int\limits_{-h/2}^{h/2} \left(\frac{\Xi_{11}(z)\bar{e}_{31b}\alpha h^3}{8\bar{\bar{\Xi}}_{33b}} \right)\left(z + \frac{h}{2} \right) dz \tag{A.23}$$

$$F_2 = -\int\limits_{-h/2}^{h/2} \left(\frac{h\Xi_{11}(z)\bar{e}_{31b}\left(1-\alpha h^2/4 \right)}{2\bar{\bar{\Xi}}_{33b}} \right)\left(z + \frac{h}{2} \right) dz \tag{A.24}$$

$$F_3 = -\int\limits_{-h/2}^{h/2} \left(\frac{\Xi_{11}(z)\bar{e}_{31b}}{\bar{\bar{\Xi}}_{33b}} \right)\left(z + \frac{h}{2} \right) dz \tag{A.25}$$

$$F_4 = \int\limits_{-h/2}^{h/2} \left\{ n\alpha(1/2-z/h)^{n-1}\left(\frac{(\bar{e}_{31t}-\bar{e}_{31b})z^3}{h} - \frac{(\bar{\Xi}_{33t}-\bar{\Xi}_{33b})h^2\bar{e}_{31b}}{8\bar{\bar{\Xi}}_{33b}} \right) + \bar{e}_{15}(z)\left(1-3\alpha z^2 \right) - 3\bar{e}_{31}(z)\alpha z^2 \right\} dz \tag{A.26}$$

$$F_5 = \int\limits_{-h/2}^{h/2} \left\{ -n(1/2-z/h)^{n-1}\left(\frac{(\bar{e}_{31t}-\bar{e}_{31b})(z-\alpha z^3)}{h} - \frac{(\bar{\Xi}_{33t}-\bar{\Xi}_{33b})\bar{e}_{31b}\left(-\frac{\alpha h^2}{4}+1 \right)}{2\bar{\bar{\Xi}}_{33b}} \right) + (\bar{e}_{15}(z)+\bar{e}_{31}(z))\left(1-3\alpha z^2 \right) \right\} dz \tag{A.27}$$

$$F_6 = \frac{\bar{e}_{31b}\bar{\Xi}_{33t}-\bar{e}_{31b}\bar{\Xi}_{33b}}{\bar{\bar{\Xi}}_{33b}} \tag{A.28}$$

$$F_7 = \frac{8}{h^2} \int\limits_{-h/2}^{h/2} \left(\bar{\Xi}_{33}(z) + n(1/2-z/h)^n\left(\bar{\Xi}_{33t}-\bar{\Xi}_{33b} \right) \right) dz \tag{A.29}$$

$$F_8 = \int\limits_{-h/2}^{h/2} \Xi_{11}(z)\left(\frac{4z^2}{h^2} - \frac{4z}{h} - 3 \right) dz \tag{A.30}$$

Appendix B

Closed circuit condition constants

$$A_1 = -\int_{-h/2}^{h/2} \bar{C}_{11}^E(z)\alpha z^3 dz \tag{B.1}$$

$$A_2 = \int_{-h/2}^{h/2} \bar{C}_{11}^E(z)\left(z - \alpha z^3\right) dz \tag{B.2}$$

$$A_3 = \frac{1}{2}\int_{-h/2}^{h/2} \left(\bar{C}_{11}^E(z) - \bar{C}_{12}^E(z)\right)\left(z - \alpha z^3\right) dz \tag{B.3}$$

$$A_4 = \frac{1}{2}\int_{-h/2}^{h/2} \left(\bar{C}_{11}^E(z) + \bar{C}_{12}^E(z)\right)\left(z - \alpha z^3\right) dz \tag{B.4}$$

$$A_5 = \int_{-h/2}^{h/2} \bar{C}_{11}^E(z) dz \tag{B.5}$$

$$A_6 = \frac{1}{2}\int_{-h/2}^{h/2} \left(\bar{C}_{11}^E(z) - \bar{C}_{12}^E(z)\right) dz \tag{B.6}$$

$$A_7 = \frac{1}{2}\int_{-h/2}^{h/2} \left(\bar{C}_{11}^E(z) + \bar{C}_{12}^E(z)\right) dz \tag{B.7}$$

$$A_8 = -\int_{-h/2}^{h/2} \frac{8z\bar{e}_{31}(z)}{h^2} dz \tag{B.8}$$

$$B_1 = -\int_{-h/2}^{h/2} \bar{C}_{11}^E(z)\alpha z^3\left(z - \alpha z^3\right) dz \tag{B.9}$$

$$B_2 = \int_{-h/2}^{h/2} \bar{C}_{11}^E(z)\left(z - \alpha z^3\right) dz \tag{B.10}$$

$$B_3 = \frac{1}{2}\int_{-h/2}^{h/2} \left(\bar{C}_{11}^E(z) - \bar{C}_{12}^E(z)\right)\left(z - \alpha z^3\right)^2 dz \tag{B.11}$$

$$B_4 = \frac{1}{2}\int_{-h/2}^{h/2} \left(\bar{C}_{11}^E(z) + \bar{C}_{12}^E(z)\right)\left(z - \alpha z^3\right)^2 dz \tag{B.12}$$

$$B_5 = \int_{-h/2}^{h/2} \left(\bar{C}_{11}^E(z)\right)\left(z - \alpha z^3\right) dz \tag{B.13}$$

$$B_6 = \frac{1}{2} \int_{-h/2}^{h/2} \left(\bar{C}_{11}^E(z) - \bar{C}_{12}^E(z) \right) \left(1 - \alpha z^3 \right) dz \tag{B.14}$$

$$B_7 = \frac{1}{2} \int_{-h/2}^{h/2} \left(\bar{C}_{11}^E(z) + \bar{C}_{12}^E(z) \right) \left(z - \alpha z^3 \right) dz \tag{B.15}$$

$$B_8 = - \int_{-h/2}^{h/2} C_{55}^E(z) \left(1 - 3\alpha z^2 \right)^2 dz \tag{B.16}$$

$$B_9 = - \int_{-h/2}^{h/2} \left\{ \left(\frac{8z^2 \bar{e}_{31}(z)}{h^2} \right) \left(1 - \alpha z^2 \right) + \bar{e}_{15}(z) \left(1 - \frac{4z^2}{h^2} \right) \left(1 - 3\alpha z^2 \right) \right\} dz \tag{B.17}$$

$$D_1 = -\alpha \int_{-h/2}^{h/2} \bar{C}_{11}^E(z) z^6 dz \tag{B.18}$$

$$D_2 = \alpha \int_{-h/2}^{h/2} \bar{C}_{11}^E(z) \left(z - \alpha z^3 \right) z^3 \right\} dz \tag{B.19}$$

$$D_3 = \alpha \int_{-h/2}^{h/2} \bar{C}_{11}^E(z) z^3 dz \tag{B.20}$$

$$D_4 = -B_8 \tag{B.21}$$

$$D_5 = \alpha \int_{-h/2}^{h/2} \left\{ \frac{4\bar{e}_{31}(z)}{h} (1 - 2z/h) z^3 + \bar{e}_{15}(z) \left(\frac{4z^2}{h^2} - \frac{4z}{h} - 3 \right) \left(3\alpha z^2 - 1 \right) \right\} dz \tag{B.22}$$

$$F_1 = 0 \tag{B.23}$$

$$F_2 = 0 \tag{B.24}$$

$$F_3 = 0 \tag{B.25}$$

$$F_4 = \int_{-h/2}^{h/2} \left\{ n\alpha (1/2 - z/h)^{n-1} \left(\frac{(\bar{e}_{31t} - \bar{e}_{31b}) z^3}{h} \right) + \right.$$
$$\left. \bar{e}_{15}(z) \left(1 - 3\alpha z^2 \right) - 3\bar{e}_{31}(z) \alpha z^2 \right\} dz \tag{B.26}$$

$$F_5 = \int_{-h/2}^{h/2} \left\{ -n(1/2 - z/h)^{n-1} \left(\frac{(\bar{e}_{31t} - \bar{e}_{31b})(z - \alpha z^3)}{h} \right) + \right.$$
$$\left. (\bar{e}_{15}(z) + \bar{e}_{31}(z)) \left(1 - 3\alpha z^2 \right) \right\} dz \tag{B.27}$$

$$F_6 = \bar{e}_{31b} - \bar{e}_{31b} \tag{B.28}$$

$$F_7 = \frac{8}{h^3} \int_{-h/2}^{h/2} \left(h\bar{\Xi}_{33}(z) - n(1/2 - z/h)^{n-1}(\Xi_{33t} - \bar{\Xi}_{33b})z \right) dz \tag{B.29}$$

$$F_8 = -\int_{-h/2}^{h/2} \bar{\Xi}_{11}(z)\left(1 - \frac{4z^2}{h^2} \right) dz \tag{B.30}$$

Appendix C

$$k_{11} = -A_1\left(\eta^2 + \mu^2\right)\eta \tag{C.1}$$

$$k_{12} = A_8\eta \tag{C.2}$$

$$k_{13} = -\left(A_2\eta^2 + A_3\mu^2\right) \tag{C.3}$$

$$k_{14} = -A_4\eta\mu \tag{C.4}$$

$$k_{15} = -\left(A_5\eta^2 + A_6\mu^2\right) \tag{C.5}$$

$$k_{16} = -A_7\eta\mu \tag{C.6}$$

$$k_{21} = -A_1\left(\eta^2 + \mu^2\right)\mu \tag{C.7}$$

$$k_{22} = A_8\mu \tag{C.8}$$

$$k_{23} = -A_4\eta\mu \tag{C.9}$$

$$k_{24} = -\left(A_3\eta^2 + A_2\mu^2\right) \tag{C.10}$$

$$k_{25} = -A_7\eta\mu \tag{C.11}$$

$$k_{26} = -\left(A_6\eta^2 + A_5\mu^2\right) \tag{C.12}$$

$$k_{31} = -B_1\left(\eta^3 + \eta\mu^2\right) + B_8\eta \tag{C.13}$$

$$k_{32} = B_9\eta \tag{C.14}$$

$$k_{33} = -\left(B_2\eta^2 + B_3\mu^2\right) + B_8 \tag{C.15}$$

$$k_{34} = -B_4\eta\mu \tag{C.16}$$

$$k_{35} = -\left(B_5\eta^2 + B_6\mu^2\right) \tag{C.17}$$

$$k_{36} = -B_7\eta\mu \tag{C.18}$$

$$k_{41} = -B_1\left(\mu^3 + \mu\eta^2\right) + B_8\mu \tag{C.19}$$

$$k_{42} = B_9\mu \tag{C.20}$$

$$k_{43} = -B_4\eta\mu \tag{C.21}$$

$$k_{44} = -\left(B_3\eta^2 + B_2\mu^2\right) + B_8 \tag{C.22}$$

$$k_{45} = -B_7\eta\mu \tag{C.23}$$

$$k_{46} = -\left(B_6\eta^2 + B_5\mu^2\right) \tag{C.24}$$

$$k_{51} = D_1\left(\mu^4 + 2\mu^2\eta^2 + \eta^4\right) - D_4\left(\mu^2 + \eta^2\right) + P_1\eta^2 \tag{C.25}$$

$$k_{52} = -D_5\left(\mu^2 + \eta^2\right) \tag{C.26}$$

$$k_{53} = D_2\left(\mu^2 + \eta^2\right)\eta - D_4\eta \tag{C.27}$$

$$k_{54} = D_2\left(\mu^2 + \eta^2\right)\mu - D_4\mu \tag{C.28}$$

$$k_{55} = D_3\left(\mu^2 + \eta^2\right)\eta \tag{C.29}$$

$$k_{56} = D_3\left(\mu^2 + \eta^2\right)\mu \tag{C.30}$$

$$k_{61} = F_1\left(\mu^4 + 2\mu^2\eta^2 + \eta^4\right) - F_4\left(\mu^2 + \eta^2\right) \tag{C.31}$$

$$k_{62} = -F_7\left(\mu^2 + \eta^2 - 1\right) \tag{C.32}$$

$$k_{63} = F_2\left(\mu^2 + \eta^2\right)\eta - F_5\eta \tag{C.33}$$

$$k_{64} = F_2\left(\mu^2 + \eta^2\right)\mu - F_5\mu \tag{C.34}$$

$$k_{65} = F_3\left(\mu^2 + \eta^2\right)\eta - F_6\eta \tag{C.35}$$

$$k_{66} = F_3\left(\mu^2 + \eta^2\right)\mu - F_6\mu \tag{C.36}$$